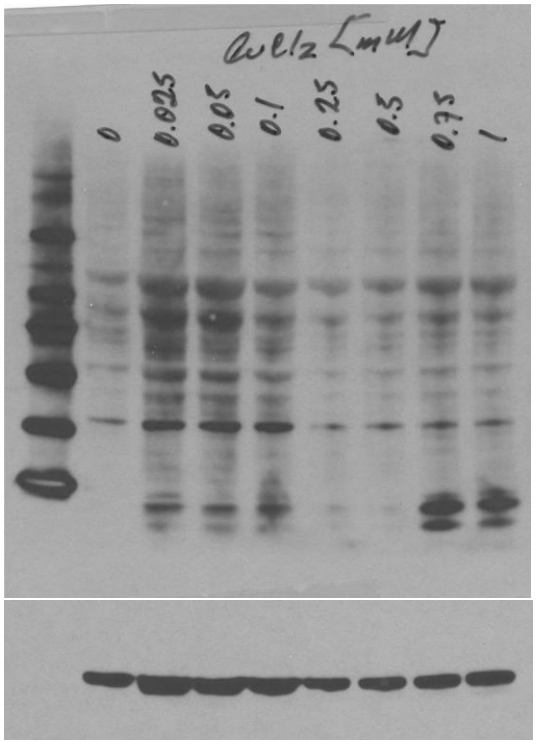

Supplementary Figure 1. Unmodified WB from **Figure 1D** (uncropped)**.** Upper film was developed using anti-cleaved caspase 3 (*) (Asp175), while bottom image was obtained after the same film was reprobed and developed with anti-β-actin antibody.

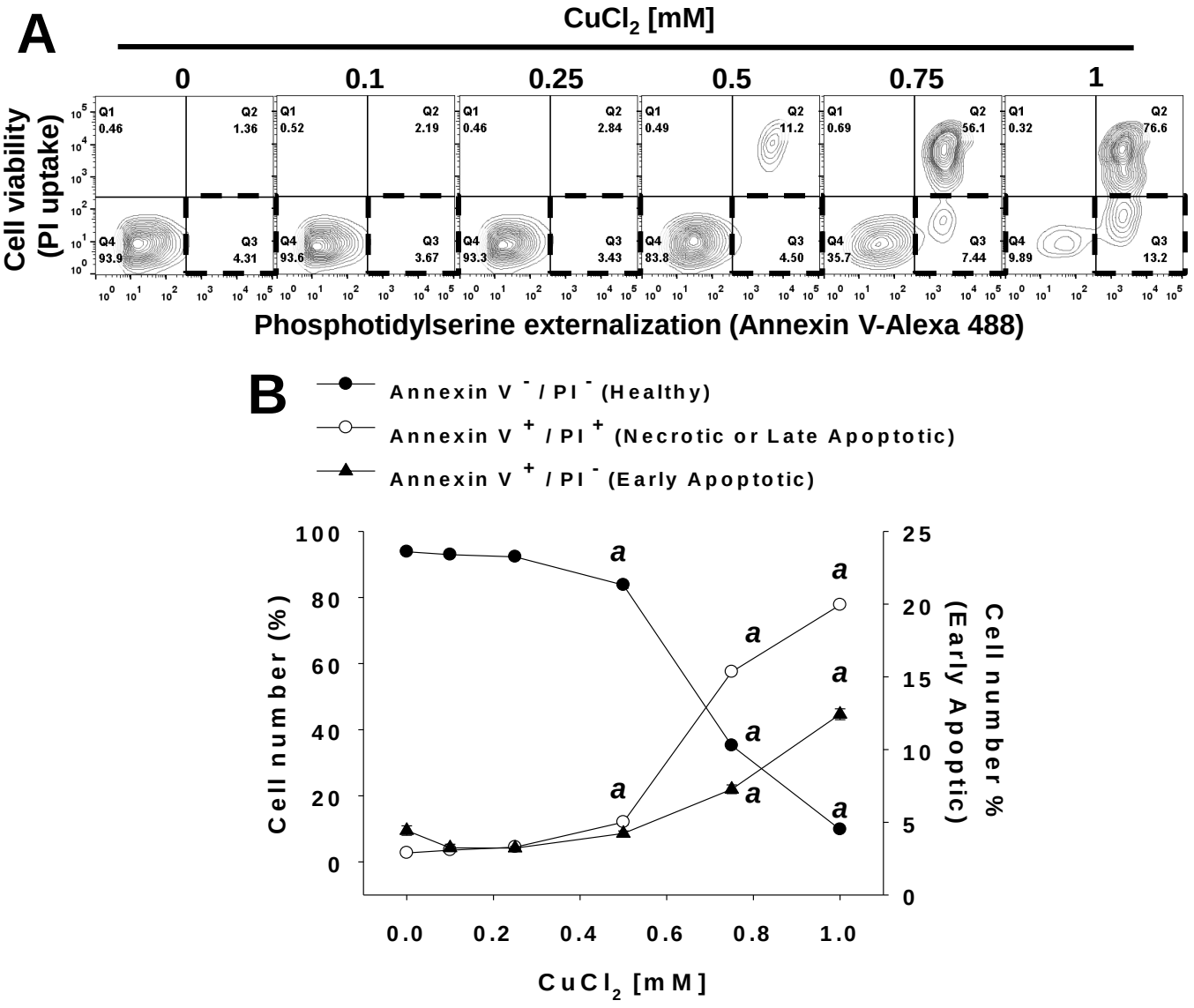

Supplementary Figure 2. Apoptosis induced by $CuCl_2$ (48 h) was evaluated by simultaneous staining with PI and Annexin V-Alexa 488 (externalized phosphatidylserine). Results are represented as two-dimensional 5% probability contour plots displaying cell death (PI uptake) vs externalized phosphatidylserine (Annexin V) (**A**) . The number of viable "healthy' cells (Annexin V- / PI-, quadrant 4 [*Q4*]), early apoptotic cells (Annexin V+ / PI-, *Q3*), and late apoptotic (secondary necrosis, Annexin V+ / PI+, *Q1* and *Q2*) cells was quantified and represented in scatter plots in **B**. % of early apoptotic cells is represented with an independent y axis (*left*). Data represent means ± SE of at least n = 3. Kruskal-Wallis one-Way ANOVA on Ranks, Student-Newman-Keuls *post hoc* test, $^{a}p<0.05$ vs 0 mM $CuCl_2$ for each population category.

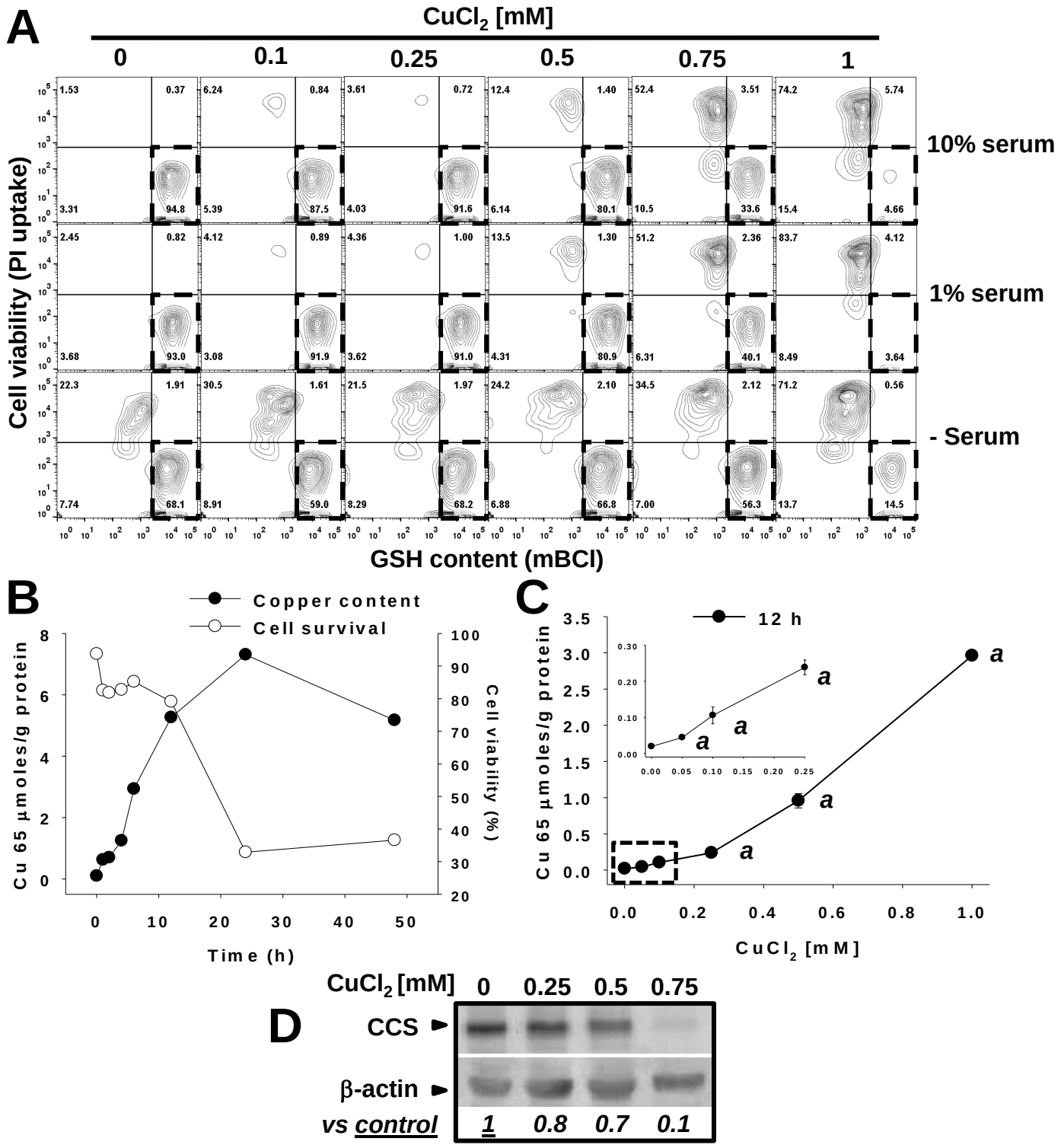

Supplementary Figure 3. In **A**, the effects of FBS on cell death induced by $CuCl_2$ (48 h) were evaluated by simultaneous staining with PI (cell death) and mBCl (GSH content). Results are represented as two-dimensional 5% probability contour plots displaying changes in the population of cells with increased PI uptake or GSH depletion (**A**). Healthy cells (PI- and high mBCl fluorescence) are depicted in *broken line regions*. In **B-C**, changes in intracellular Cu content induced by $CuCl_2$ were determined by ICP-MS. Data was normalized by protein content and quantified in **C** representing means ± SE of n =3. *Inset* represents a magnification of data in the *broken line squares*. Kruskal-Wallis one-Way ANOVA on Ranks, Student-Newman-Keuls *post hoc* test, $^{a}p<0.05$ vs 0mM $CuCl_2$. In **D**, changes in CCS protein levels induced by $CuCl_2$ were evaluated by WB. Numbers (*italics*) represent the densitometry analysis of CCS normalized to β-actin signal with respect to control.

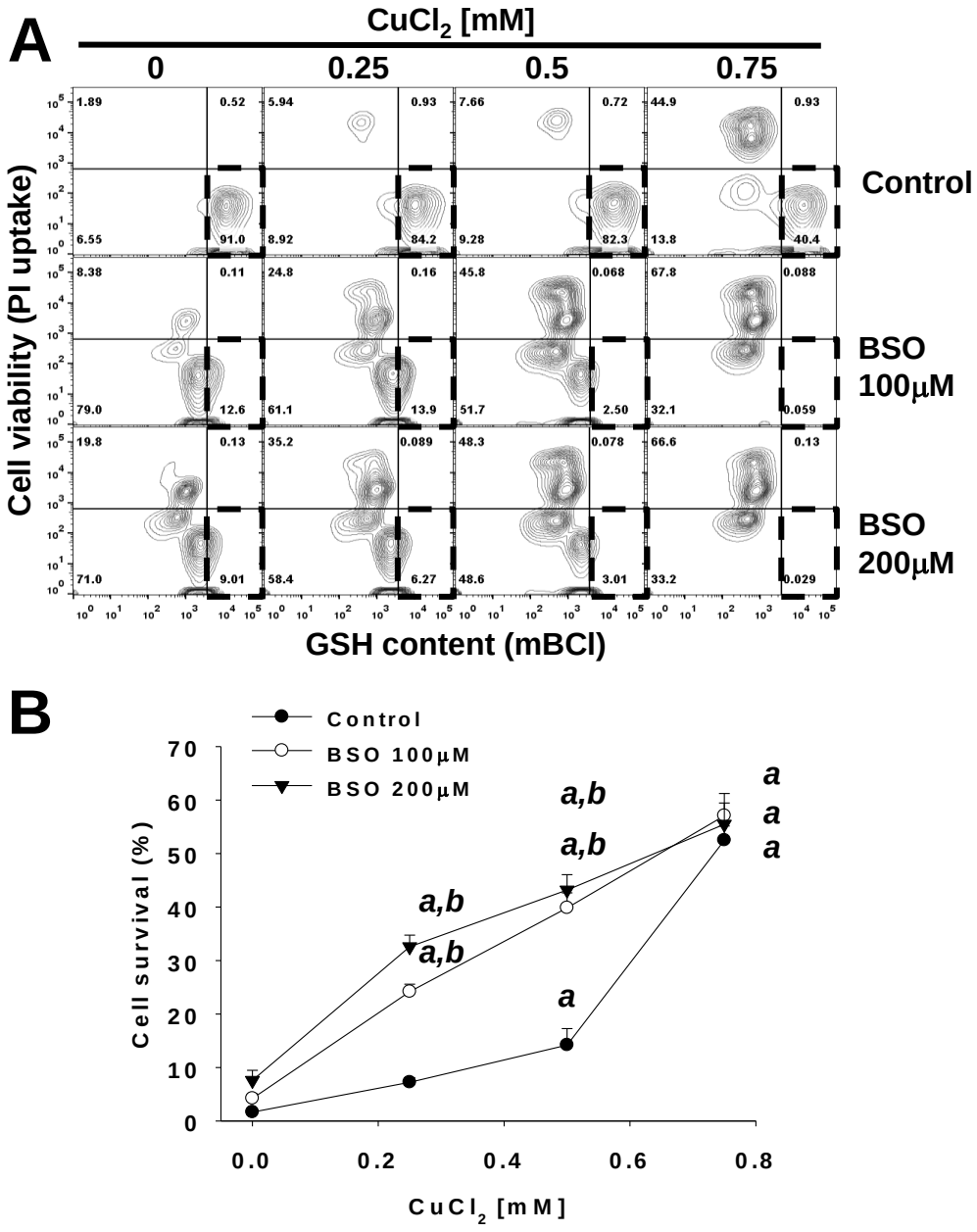

Supplementary Figure 4. Cells where incubated with the indicated concentration of BSO for 24 h prior to $CuCl_2$ treatment (BSO remained throughout the experiment). In **A**, cell death induced by $CuCl_2$ (48 h) was evaluated by simultaneous staining with PI (cell death) and mBCl (GSH content). Results are represented as two-dimensional 5% probability contour plots displaying changes in the population of cells with increased PI uptake or GSH depletion (**A**). Healthy cells (PI- and high mBCl fluorescence) are depicted in *broken line regions* and are quantified in **B.** Two-way ANOVA, Holm-Sidak *post hoc* test, $^{a}p<0.05$ *vs* 0 mM $CuCl_2$ for each category (Control, BSO 100 µM or BSO 200 µM); $^{b}p<0.05$ *vs* control at the corresponding [$CuCl_2$] tested.

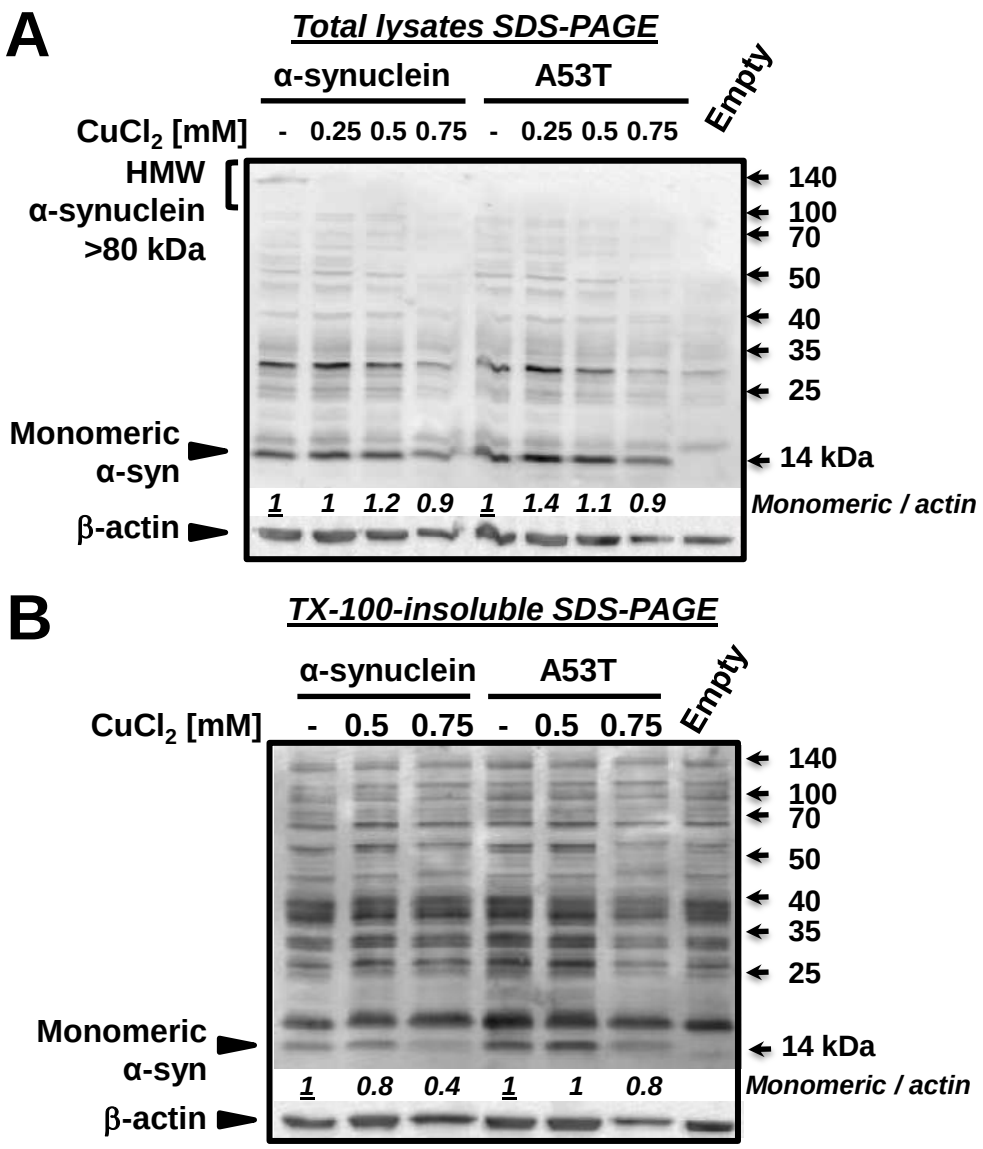

Supplementary Figure 5. Cells were transduced with Ad-Empty, Ad-α-synuclein or Ad-A53T (3 MOI). After 24 h, cells were washed and treated with $CuCl_2$ for 48 h. Total lysates (RIPA / SDS-PAGE) (**A**) and TX-100-insoluble (RIPA solubilization of post-TX-100 extracts / SDS-PAGE) fractions were isolated and analyzed as explained in Materials and Methods. α-synuclein was detected with a carboxy-terminal directed antibody. Numbers (*italics)* represent the densitometry analysis normalized to β-actin with respect to control. WB in **B** is the complete blot shown partially in **Figure 5** (*monomeric, SDS-PAGE*).

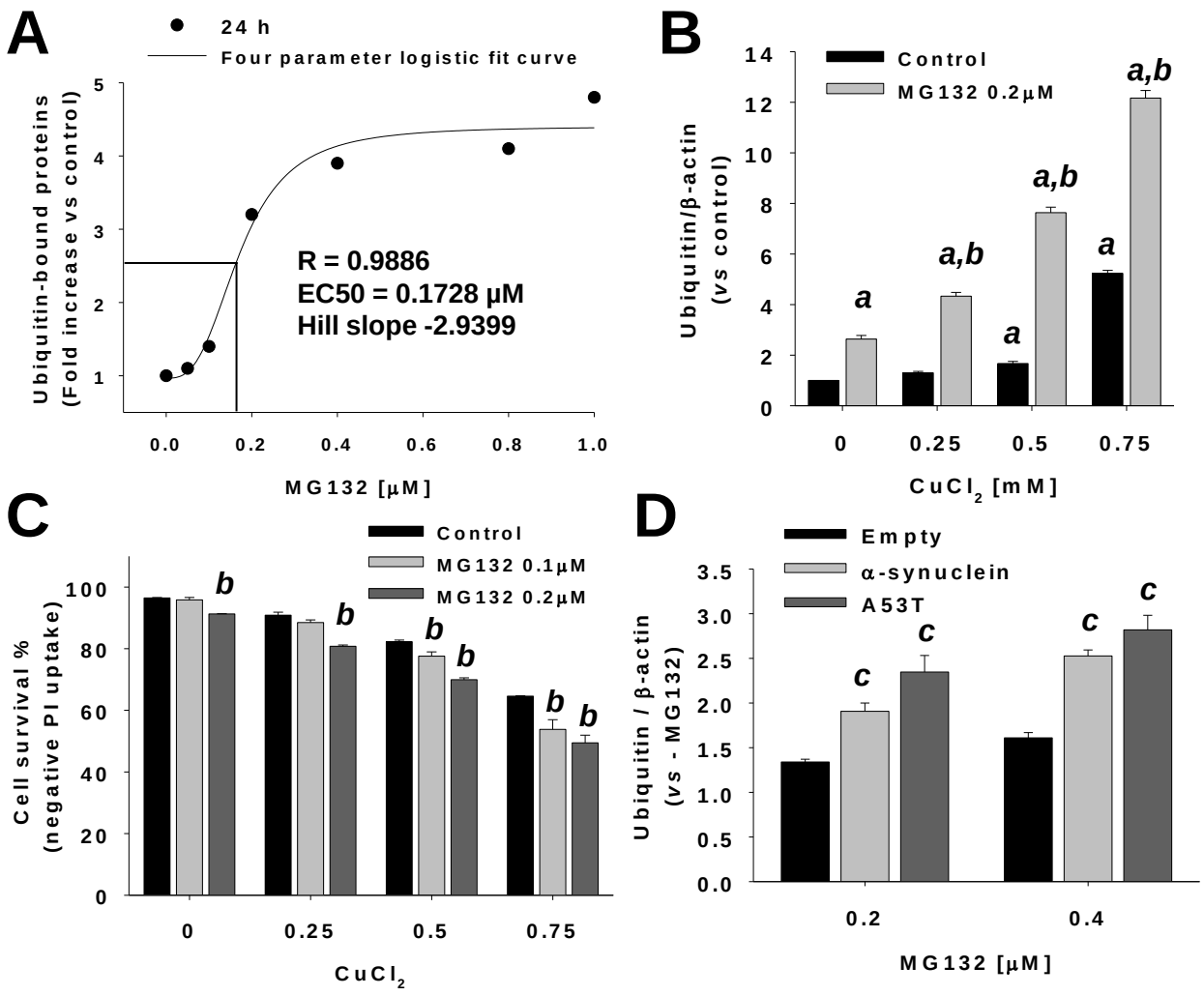

Supplementary Figure 6. In **A**, four parameter logistic fit curve for the densitometry analysis of the accumulation of ubiquitin-bound proteins induced by MG132 (**Figure 8A**, *upper dot blot*). Intersecting lines depict EC_{50} for the induced accumulation of ubiquitin-bound proteins. Data were normalized with respect to control *(see densitometry analysis in* **Figures 8A-B**). In **B** and **D**, densitometry analysis of the accumulation of ubiquitin-bound proteins induced by $CuCl_2$ (**Figures 8B)** or by overexpression of α-synuclein (WT or A53T mutant) (**Figures 8D)**, respectively, in the presence or absence of MG132. In **C**, changes in cell survival upon $CuCl_2$ treatment in the presence or absence of MG132 (48 h). Cell viability was determined by simultaneous analysis of both PI uptake and changes in intracellular GSH (mBCl) by flow cytometry as exemplified in **Figure 1A**. Viable cells were defined as cells with high intracellular glutathione levels (GSH), and PI-. %s represent means ± SE of n = 3 independent experiments. Two-way ANOVA, Holm-Sidak, $^{a}p<0.05$ *vs* -$CuCl_2$ within the corresponding category ± MG132; $^{b}p<0.05$ *vs* - MG132 within the corresponding [$CuCl_2$]; $^{c}p<0.05$ *vs* Empty within the corresponding [MG132] category.

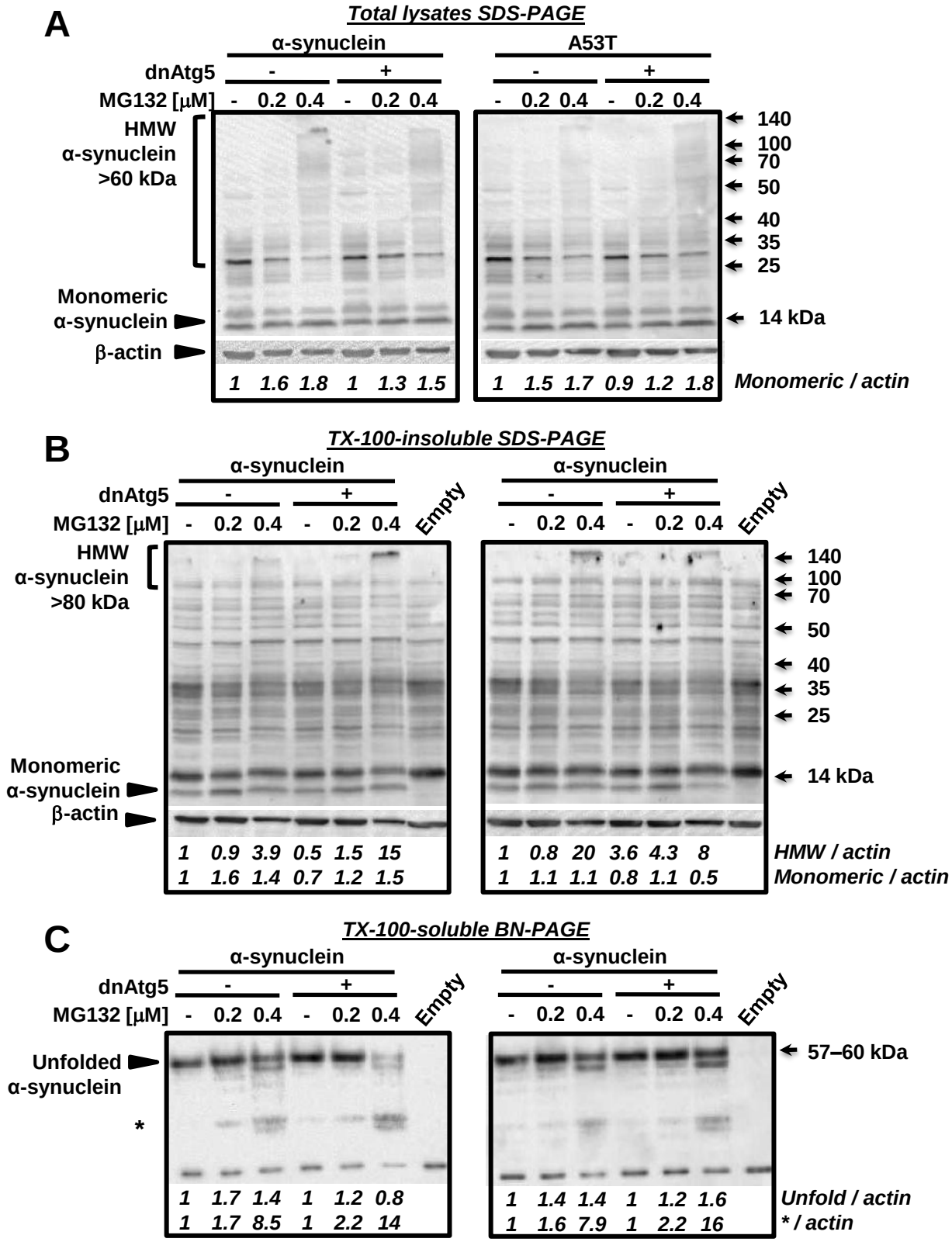

Supplementary Figure 7. Cells were transduced with Ad-Empty, Ad-α-synuclein or Ad-A53T (3 MOI). After 48 h, cells were washed and treated with 0.2 μM MG132 for 24 h. Total lysates (RIPA / SDS-PAGE) (**A**) and TX-100-insoluble (RIPA solubilization of post-TX-100 extracts / SDS-PAGE, **B**) or soluble (TX-100 / Blue Native-PAGE, **C**) fractions were isolated and analyzed as explained in Materials and Methods. α-synuclein was detected with a carboxy-terminal directed antibody. Numbers (*italics)* represent the densitometry analysis normalized to β-actin with respect to the corresponding control.

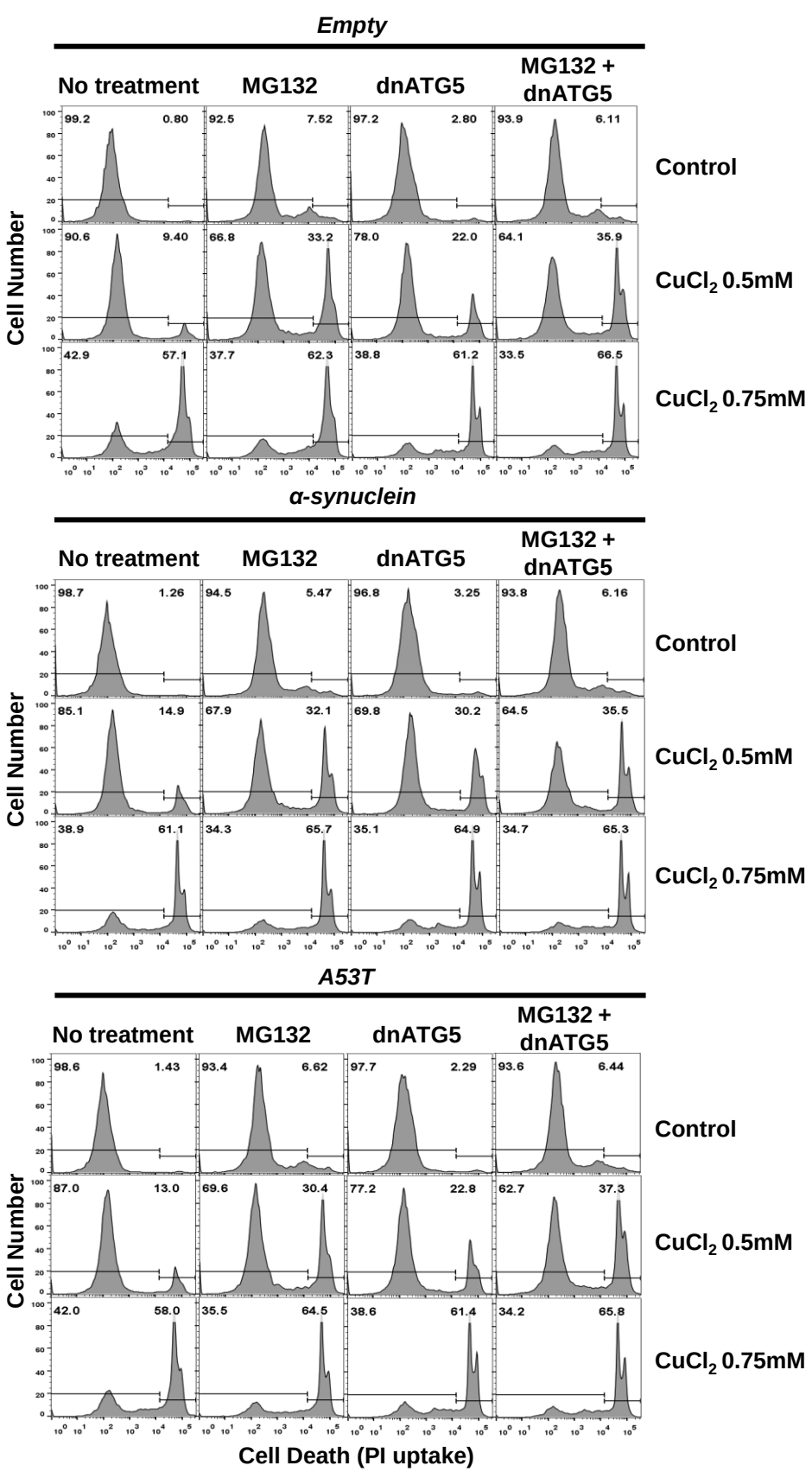

Supplementary Figure 8. Cells were transduced with Ad-Empty or Ad-dnAtg5 (1.5 MOI) and/or Ad-Empty, Ad-α-synuclein or Ad-A53T (3 MOI) for 24h, washed and then treated with or without $CuCl_2 \pm$ MG132 (0.2 μM) for 48 h before analysis. Alterations in cell viability were determined by analysis of PI uptake by flow cytometry. Viable cells are defined as cells with high PI fluorescence. %s represent the population of viable cells (*right region*) or dead cells (*left region*).

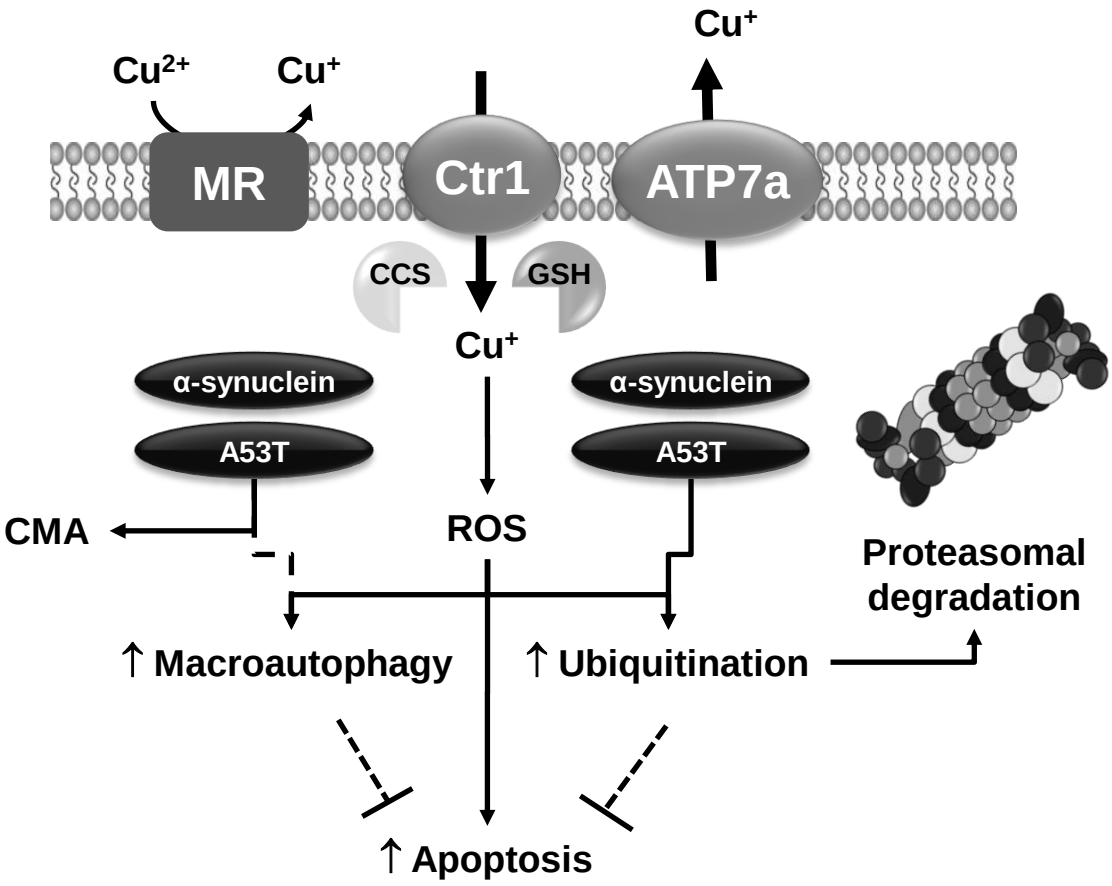

Supplementary Figure 9. WT or A53T α-synuclein overexpression stimulates Cu toxicity by modulation of protein degradation pathways. Cu-binding proteins and transporters properly handle Cu cellular homeostasis and minimize its potential detrimental effects. High-affinity Cu^{1+} import into eukaryotic cells is mediated by Ctr1/*SLC31A1*. The extracellular oxidizing environment favors equilibrium toward Cu^{2+}. Reduction of Cu^{2+} to Cu^{+} by plasma membrane metalloreductases (MR, encoded by the FRE1 and FRE2 genes in yeast (Georgatsou et al., 1997), or STEAP genes in humans (Ohgami et al., 2006)) is required to efficiently transport extracellular Cu across the plasma by Ctr1, which mediates the movement of Cu^{+} and not Cu^{2+} (Lee et al., 2002; Telianidis et al., 2013). On the other hand, P-type ATPase transporters ATP7AB, transport Cu^{+} or Cu^{2+} from the cytosol across cellular membranes, thus decreasing cytosolic Cu concentration. Intracellular Cu concentrations are tightly controlled by chelating systems for Cu, which include methalothioneins, chaperones (CCS), and GSH. In this work we demonstrated, that Cu can exert a synergistic toxic effect with either WT or A53T α-synuclein independent from α-synuclein aggregation. Cu toxicity was associated with the induction of apoptosis and was directly linked to intracellular GSH levels and modulation of Cu transport demonstrating the specific role of changes in intracellular Cu levels. This synergistic toxic effect of Cu and α-synuclein seems to be mediated by an increase "stress load" to protein degradation mechanisms, primarily the UPS, but to a lesser extent autophagy. This was revealed by the fact that impairment in proteasomal activity with MG132 stimulated the toxicity of $CuCl_2$ and α-synuclein. In contrast, inhibition of Atg5-dependent macroautophagy stimulated $CuCl_2$-induced cell death, but did not affect cells overexpressing either form of α-synuclein. Our findings do not discard a potential compensatory role of CMA, which is known to counteract the dysfunction in macroautophagy. In addition, we suggest that the toxic effect of Cu and α-synuclein might be associated with alterations in the native state of the monomer.

REFERENCES IN THE SUPPLEMENTARY INFORMATION

Georgatsou E, Mavrogiannis LA, Fragiadakis GS, Alexandraki D. The yeast Fre1p/Fre2p cupric reductases facilitate copper uptake and are regulated by the copper-modulated Mac1p activator. J Biol Chem. 1997;272:13786-92.

Lee J, Pena MM, Nose Y, Thiele DJ. Biochemical characterization of the human copper transporter Ctr1. J Biol Chem. 2002;277:4380-7.

Ohgami RS, Campagna DR, McDonald A, Fleming MD. The Steap proteins are metalloreductases. Blood. 2006;108:1388-94.

Telianidis J, Hung YH, Materia S, Fontaine SL. Role of the P-Type ATPases, ATP7A and ATP7B in brain copper homeostasis. Front Aging Neurosci. 2013;5:44.